Detailed Characterization of the 1087 MeV/nucleon ^{56}Fe Beam Used for Radiobiology at the AGS

C. Zeitlin, L. Heilbronn, J. Miller
Lawrence Berkeley National Laboratory, Berkeley, California 94720

Keywords: physics, dosimetry, radiobiology, heavy ions, fragmentation, AGS, Bragg Curve

ABSTRACT We report beam characterization and dosimetric measurements made using a ^{56}Fe beam extracted from the Brookhaven National Laboratory Alternating Gradient Synchrotron with a kinetic energy of 1087 MeV/nucleon. The measurements reveal that the depth-dose distribution of this beam differs significantly from that obtained with a 600 MeV/nucleon iron beam used in several earlier radiobiology experiments at the Lawrence Berkeley Laboratory's BEVALAC. We present detailed measurements of beam parameters relevant for radiobiology, including track- and dose-averaged LET, fragment composition, and LET spectra measured behind sample holders used in biology irradiations. We also report measurements of fluence behind three depths (1.94, 4.68, and 9.35 g cm^{-2}) of polyethylene targets with the 1087 MeV/nucleon beam, and behind 1.94 g cm^{-2} of polyethylene with a 610 MeV/nucleon beam delivered by the AGS. These results are compared to earlier measurements with the 600 MeV/nucleon beam at the BEVALAC.

INTRODUCTION

It has long been recognized that irradiation by high-energy heavy ions in the Galactic Cosmic Rays (GCR) may affect the health of humans on long-duration spaceflight both inside and outside the geomagnetosphere, and many significant issues relating to these risks remain unresolved (1). Because iron ions are the most densely ionizing particles which are present in significant numbers in the GCR, there has been considerable interest in understanding their transport through matter and their biological effects. Accordingly, numerous radiobiology experiments using iron ions were conducted at the Lawrence Berkeley Laboratory's BEVALAC with typical extracted beam energies of 400 to 600 MeV/nucleon. (A partial list of publications relating to these experiments is given here as Refs. 2-6; further references are contained therein.) After the shutdown of the BEVALAC in early 1993 (with the last radiobiology experiments in December 1992), there was no facility in the U.S. for radiobiology experiments with high energy heavy ions until October 1995, when a 1087 MeV/nucleon (at extraction) iron beam became available for radiobiological use at the Brookhaven National Laboratory's Alternating Gradient Synchrotron (AGS). A beamline modeled on one used for similar irradiations at the BEVALAC was constructed at the AGS, and a dosimetry system incorporating many elements of the BEVALAC system was implemented. Several radiobiology experiments and one physics experiment (7) were performed on this beamline in 1995; additional experiments were performed in October 1996. At the end of the 1996 run, a 610 MeV/nucleon ^{56}Fe beam was extracted from the AGS and transported to the experimental area, with the primary purpose of establishing that such a beam could be reliably delivered. Some physics measurements and biology irradiations were performed with this beam as well.

In this paper, we focus primarily on some properties of the 1087 MeV/nucleon AGS iron beam which are important for the interpretation of the biology experiments. (Throughout, linear energy transfer in water — formally, LET_∞ — is abbreviated to LET.) We present beam characterization data consisting of measurements of: beam energy; fluence vs. LET as seen at the upstream edge of a biological sample; dose

vs. LET; track- and dose-averaged LET (8) measured behind several sample holders used in biology irradiations; radial beam uniformity; and the Bragg curve. Finally, we present fragment fluences behind polyethylene targets, and compare them to similar data obtained at the BEVALAC.

MATERIALS AND METHODS

DOSIMETRY SYSTEM

Measurements of the physical characteristics of the AGS iron beams were performed with two separate systems. The conventional dosimetry system consisted of three parallel-plate ionization chambers (IC1, IC2 and IC3), used in conjunction with a variable-depth water column. The two commonly-used setups of the IC's on the beamline are shown schematically in Fig. 1a and Fig. 1b. In the irradiation mode, the IC's were used to monitor the dose received by biological samples. Each IC has two gas volumes, each 1.3 cm deep, which are filled with dry nitrogen at a pressure very slightly above atmospheric pressure. In the upstream volume, ionization electrons are collected on a foil divided into quadrants, while in the downstream volume, they are collected on a foil that consists of a series of concentric rings. The gas volumes are separated by a central, unsegmented high-voltage foil which is held at -1500V potential, while the collector foils are held at ground potential. Electrons are liberated in the gas by the passage of charged particles; the quantity of charge collected on a given ring or quadrant is converted to a series of logic pulses by means of recycling integrators (one integrator channel per quadrant or ring), with one pulse output per 10 picocoulombs input. The recycling integrator output for a given channel is thus directly proportional to the absorbed dose in the gas volume adjoining the ring or quadrant to which it is connected. Proportionality constants which convert this dose to the corresponding dose in water[1] have been calculated separately for each ring, and are applied in real-time by a computer which provides updating displays and controls the cutoff signal to the accelerator. A final correction factor — typically around 8% — is applied to bring the IC dose calculated by this method into agreement with the dose measured by a Far West thimble chamber (an "egg" chamber). The thimble chamber is calibrated by the manufacturer by comparing the chamber's response to the response of a similar chamber calibrated at the National Institute of Standards and Technology.

The real-time readout from the quadrants is used to adjust the beam position; the readout of the rings provides pulse-to-pulse monitoring of the uniformity of the radial dose distribution. (Higher resolution uniformity monitoring is done by means of x-ray films placed in the beam and read out off-line.) An additional function of the IC's is the measurement of the Bragg curve (see Fig. 1b), which is obtained by taking the ratio of charge collected in a chamber placed downstream of the water column (IC3) to the charge collected in a chamber upstream of the column (IC1), as a function of depth of water. This ratio gives a characteristic peak when the water column depth is near the nominal range of the beam particles.

SILICON DETECTOR SYSTEM

A stack of silicon detectors, used primarily for fragmentation measurements [see Ref. (7)], was used for several beam characterization measurements as well. This system was previously used at the BEVALAC (9,10). These detectors are considerably more sensitive than the IC's, and are also subject to radiation damage at the fluxes used in the radiobiology irradiations done on this beamline. Beam flux is therefore reduced by roughly three orders of magnitude compared to the lowest flux used in irradiation of biological samples. At such low fluxes, the IC's do not record any useful information and are not

used, and although they are left on the beamline, they are placed well downstream of the silicon detectors so as to reduce backscatter.

A trigger (the definition of which can be varied, see below) causes the readout electronics to sample the peak of the signal (which is proportional to deposited energy ΔE) from each detector; these values are written to disk for every trigger. For any detector, ΔE is proportional to the sum of the square of the charges of the particles that hit it, i.e., the detectors measure an effective charge $Z_{eff}^2 = \sum_i Z_i^2$ on each event. This approximation is good as long as the particles all have similar velocities. If only a single particle is present, as was the case for the majority of events reported here, there is no complication. Also, if the charge of one particle (*e.g.*, a heavy fragment with charge close to that of the primary iron) is much greater than that of any other particles present, the heavy fragment dominates the effective charge, even if the lighter particles are at somewhat lower velocity than the heaviest particle.

1995 Configuration of Silicon Detectors

The arrangement of the detectors on the beamline for the 1995 run is shown in Figure 2a; this setup was designed for fluence and cross section measurements, and was not optimized for beam characterization. The trigger for the 1995 data required a coincidence of particles in T1 and T2 (both 300 μm thick silicon detectors with active areas of 300 mm^2), with thresholds set so that the trigger did not fire if the incident particle had an LET below about 20 keV/μm. For measuring cross sections, which are determined by normalizing to the number of incident iron ions, this threshold is much lower than necessary; however, for characterization, the threshold cut-off is a deficiency. Following T1 and T2 were a pair of 1 mm thick position-sensitive silicon detectors (PSD1Y and PSD1X), oriented so as to provide y and x position data. These detectors also yield signals proportional to ΔE. A similar pair, PSD2Y and PSD2X, was placed downstream of the target position; the ΔE signals from these detectors were used in the analysis of fluences behind polyethylene targets presented below. Four 3 mm-thick silicon detectors (denoted d3mm1, d3mm2, etc.) with active areas of 450 mm^2 were placed downstream of PSD2X. In the off-line analysis of these data, events were selected in which T1, T2, PSD1Y and PSD1X all had ΔE signals consistent with a single iron ion incident on these detectors, and passing through them intact to be incident on the upstream face of the target. The fluence spectra seen in the PSD2 detectors for this category of events is thus easily normalized to a single incident iron particle.

1996 Configuration-Beam Characterization

For a portion of the 1996 run, the beamline configuration of silicon detectors was altered specifically for beam characterization, as shown in Fig. 2b. The trigger was modified so that the readout of detectors was initiated by a coincidence of hits in d3mm1 and d3mm2, with the thresholds set much lower than the corresponding thresholds in T1 and T2 in 1995, so that incident particles over the entire LET range were detected.

1996 Configuration-600 MeV/nucleon Beam

Data were obtained behind several different targets, including polyethylene, with the 600 MeV/nucleon iron beam; the detectors were positioned as indicated by Fig. 2c. A single 300 μm-thick detector, T1, was placed in the most-upstream position, and was used to define the trigger. Just downstream of T1, but upstream of the target, was a 3 mm-thick detector, d3mmU. In the off-line data analysis, signals from these detectors were

both required to be consistent with a single incident iron particle passing through and striking the upstream face of the target, again simplifying the normalization of the fluence spectra seen in the detectors downstream of the target.

Determination of LET from $\Delta E/\Delta x$ in Silicon

For a given particle type and velocity, the ratio between LET and $\Delta E/\Delta x$ in silicon is mildly energy-dependent. For present purposes, this ratio is well-approximated by a constant, which varies by less than 0.5% over the entire range of particles encountered in the experiment, from the highest-energy iron to 200 MeV protons. Thus, in the data presented below, the LET scale is determined by multiplying the measured ΔE in silicon detectors by factors which cause the iron peaks to appear at 148 keV/μm. The factors are determined separately for each of the setups shown in Figure 2, using data taken with no sample holders or targets on the beamline.

Measurements Behind Polyethylene Targets

Polyethylene is a convenient tissue equivalent material, both because of its chemical composition (CH_2) and its ease of handling. Data were taken with slabs of polyethylene of varying thicknesses on the beamline, in the "target" positions indicated in Figures 2a and 2c. These data can be combined with data taken behind pure carbon targets to extract fragment production cross sections in hydrogen targets, as in Ref. (7). For present purposes, measurements behind polyethylene also yield insight into the depth-dose distribution in water, illustrate the nature of the mixed radiation fields seen at depth in tissue, and allow for comparisons to model calculations.

Table I identifies the data sets collected behind polyethylene targets at the BEVALAC and AGS. The configuration of the detectors on the beamline at the BEVALAC made it difficult to determine the proper normalization, and only a single low-statistics run was taken with no target. These "target-out" data are needed for background subtraction. In contrast, the configurations used at the AGS (Figs. 2a for data sets C, E and F, and 2c for data set B) make normalization straightforward by allowing for particle identification upstream of the target, so that in the off-line analysis, data selection cuts can guarantee that a single iron particle triggered the event. Also, at the AGS, high-statistics target-out runs were taken.

In addition to the simpler normalization method for the AGS data, identification of particle species in the AGS data is also more straightforward than in the BEVALAC data.[2] Details of the particle identification technique used in analysis of the AGS data can be found in Ref. (7); the technique used in analysis of the BEVALAC data was described in considerable detail in Ref. (9). In all our data analysis, each event is considered to be due to a single ion of a particular species, with the goal being to identify the species and with no attempt made to distinguish between isotopes of the same species. While the techniques used at the BEVALAC and AGS are different, they were shown in Ref. (9) to yield mutually consistent results.

Corrections for Background

We limit these data samples to events in which a single iron particle is incident on the target. Ideally, under this condition, data taken without a target would yield spectra consisting of 100% iron and nothing else in the downstream detectors. But due to materials on the beamline and imperfections in the data analysis methods, this is not the case and corrections to the spectra measured behind targets must be applied. The corrected fluence[3] of iron particles seen behind a target is given by:

$$\phi_{Fe}(\text{corrected}) = \phi_{Fe}(\text{observed}) / \phi_{Fe}(\text{target - out})$$

and for fragments of charge Z:

$$\phi_Z(\text{corrected}) = \phi_Z(\text{observed}) - \phi_Z(\text{target - out})\phi_{Fe}(\text{corrected})$$

.

The corrected fluence of iron particles is related to the mean free path λ by

$$\lambda = \frac{-x}{\log(\phi_{Fe}(\text{corrected}))}$$

where *x* is the target depth.

Corrections for Unequal Target Depths

The corrected fragment yields defined above sum to $1 - \phi_{Fe}(\text{corrected})$, since (effectively) one particle is detected per event. For a small variation in areal density of the target (ρx), and ignoring secondary and higher-generation interactions, it can be shown that, for a given Z, $\phi_Z \rightarrow \phi_Z + \delta\phi_Z$ where

$$\frac{\delta\phi_Z}{\phi_Z} = \frac{\delta(1 - \phi_{Fe})}{(1 - \phi_{Fe})}.$$

That is, the fractional change in the fluence of any fragment species is equal to the fractional change in the total fragment fluence. We use these relationships to adjust the 1.82 and 4.55 g cm^{-2} fluences so that they are equivalent to the 1.94 and 4.68 g cm^{-2} fluences, respectively. These corrections amount to 3.2% for the 1.82 g cm^{-2} data and 0.6% for the 4.55 g cm^{-2} data.

Corrections for Acceptance

Because the d3mm detectors used for particle identification in data sets A, B and D had small acceptance, the measured fluences must be corrected; we use Goldhaber's statistical model of fragmentation (11) with parameters determined by Tripathi and Townsend (12) to calculate angular distributions and hence acceptance as a function of Z, beam energy, and angle subtended by the detectors. The results for those data sets have been corrected according to this model. Data sets C and E were obtained with a larger acceptance (3.5°), and no corrections are needed (i.e., the model predicts 100% acceptance) for the $Z \geq 12$ fluences presented here.

RESULTS

MEASUREMENTS OF BEAM ENERGY - 1995

The nominal energy of the beam at AGS extraction was 1087 MeV/nucleon. The beam traversed several materials before entering the experimental area through a thin exit window which marked the end of the vacuum line. (In the following, we refer to the point just downstream of this final window as "at the exit window.") The Bragg curve for 1995, shown in Fig. 3, has a peak in the ionization ratio at 27.8-27.9 cm of water, depending on which ring of the ionization chamber is considered. In interpreting the location of the peak, it is necessary to account for the entrance and exit windows on the water column, which in total consist of 1.63 g cm^{-2} of water-equivalent acrylic. Also, the beam traversed approximately 2 meters of air, or about 0.24 g cm^{-2}, before reaching the water column entrance window. Thus the true range of the beam was approximately 29.7 cm of water, which, according to standard range-energy tables (13), corresponds to a beam energy of about 1060 MeV/nucleon at the exit window. In a separate calculation[4], we have used a heavy ion transport model (15, 16) to simulate the passage of an iron particle through the materials between the point of extraction from the AGS and the exit window in the experimental area. For an extraction energy of 1087 MeV/nucleon, this calculation predicts an energy of 1064

MeV/nucleon, in excellent agreement with the energy determined from the Bragg peak.

An independent measurement of beam energy was made by means of off-line analysis of data from silicon detectors d3mm1, 2, 3 and 4. Pulse heights were converted into measurements of deposited energy, ΔE, using a standard calibration scheme (see Ref. (9) for details). We define the following quantity for each of the d3mm detectors:

$$\text{Ratio}(i^{\text{th}}\ \text{detector}) = \frac{\Delta E_i(\text{Iron peak, target in})}{\Delta E_i(\text{Iron peak, target out})}$$

where the peaks were found by using events which met stringent selection criteria to insure that the entire detector stack was traversed by a single iron ion. The resulting histogram for each detector was then fit with a Gaussian distribution to the central bins. Calculations with our transport model show that, with a thick target, the ratios are very sensitive to the energy of the beam at the exit window. Data taken behind a 10.4 cm polyethylene target are in excellent agreement with the calculation using a beam energy of 1087 MeV/nucleon at extraction, which implies an energy of 1064 MeV/nucleon at the exit window and 1055 MeV/nucleon at the biology sample position. Varying the extraction energy in the calculation — or varying the simulated materials assumed to be upstream of the exit window — yields ratios which do not agree with the data.

The two methods yield results that are mutually consistent, and show that iron ions at the exit window have an LET of 147.8 keV/μm. Calculations show that after traversing 2 meters of air and the 3 ionization chambers — to reach the typical biological sample location — the LET of iron ions is 148.1 keV/μm.

MEASUREMENTS OF BEAM ENERGY - 1996

The Bragg curve data for 1996 have a peak in the ionization ratio at 27.4 cm of water, about 5 mm less than was found in the 1995 data. Taking into account the additional materials on the beam line, this corresponds to a range in water of 29.2 cm. From Ref. (13), we find that this range corresponds to a kinetic energy of 1053 MeV/nucleon, about 7 MeV/nucleon lower than was found by this method in the 1995 data. The difference is attributable to the presence of beam-monitoring detectors upstream of the vacuum exit window which were taken out during the 1995 run but which were in the beamline during the 1996 run. Calculations show that the slightly lower beam energy has a negligible effect on the LET for iron particles, which remains very close to 148 keV/μm.

The beam energy measurement using the ratio of ΔE's in silicon detectors was repeated with 1996 data. Again, the results favor an extraction energy of 1087 MeV/nucleon, which in turn leads to a predicted energy of 1058 MeV/nucleon at the exit window, 6 MeV/nucleon lower than was found by this method in the 1995 data. This value is in excellent agreement with that determined from the Bragg curve.

FLUENCE AND DOSE VS. LET

Since the 1995 data were subject to a 20 keV/μm trigger threshold, we use the 1996 data to determine fluence, dose and integrated dose, all as functions of LET, for the beam at the exit window. Both years' data are used to determine these same quantities behind sample holders; corrections for the trigger threshold effects are made to the earlier data.

Fluence vs. LET

Figure 4a shows ϕ vs. LET obtained by taking the sum of deposited energies in d3mm1 and d3mm2, with data obtained in 1996. The spectrum corresponds closely to what would be seen at the upstream edge of a sample holder. In the off-line data analysis, two event selection criteria were applied to obtain this spectrum. We require

that: (1) the same particle hit each detector and traversed both intact; (2) the ΔE in each detector was significantly above zero. Energy-loss calculations show that a beam-velocity proton will deposit about 1.3 MeV in a detector of 3 mm thickness; since this is the lowest plausible ΔE for a valid beam particle in this experiment, we set the low-end cuts in the pulse-height spectra to correspond to 1.0 MeV in d3mm1 and d3mm2.

In Fig. 4a, a very large peak of iron events stands out, even with a logarithmic scale on the vertical axis. The events with ΔE below the iron peak are presumably fragments created when an iron ion interacts in material upstream in the beamline; lighter ions produced in the accelerator which survive transport to the experimental area also populate this region. The track-averaged LET is 112 keV/μm; this value is strongly influenced by the peak at low LET, and is sensitive to details of the cuts used to define the data sample. That is, small variations in the definitions of the cuts used in the analysis produce corresponding variations — at the level of about ±3% — in the values of track-averaged LET obtained. Considering that there is no *a priori* correct choice of cuts, we assign a systematic uncertainty of ±3% to these values. The dose-averaged LET is found to be 145 keV/μm, and this quantity is much less sensitive (with observed variations on the order of ±1%) to details of the cuts.[5]

Dose vs. LET

The fluence spectrum shown in Fig. 4a was used to generate a plot of dose (in arbitrary units) as a function of LET, by multiplying the fluence in each bin by the value of LET at the center of the bin and entering the product into a new histogram, which was then normalized to have an integral of 1. The result is shown in Figure 4b. Clearly, although there is a large peak in the fluence spectrum at low LET, those particles do not contribute much to the dose. This point is further illustrated in Fig. 4c, in which the integral of Fig. 4b (again normalized to 1) is shown as a function of LET. Less than 3% of the dose is attributable to particles with LET < 100 keV/μm, and another 3% is attributable to particles with 100 < LET < 140 keV/μm; the remaining 94% of the dose is contributed by iron particles.

Dose- and Track-Averaged LETs Behind Sample Holders

We are interested in fluences and doses measured behind sample holders used in radiobiology experiments on the AGS beamline. Some of these data were collected in 1995, others in 1996. To correct for particles below the trigger threshold in the 1995 data, we use LET < 20 keV/μm data obtained in the 1996 run, which show that 23% of the total number of tracks were in this region (with an average LET of 3 keV/μm). Accordingly, for each sample holder for which we took data in 1995, the ϕ vs. LET spectrum was normalized so that its integral was 0.77, and the low-LET fluence spectrum was then added to the measured spectrum. The resulting spectrum is then used for calculations of all quantities of interest. (These same quantities were calculated directly from the 1996 ϕ vs. LET spectra with no corrections.)

Fluences were measured behind several sample holders used in the biology experiments. In the 1996 run, holders were placed on the beamline upstream of d3mm1 (see Fig. 2b); in the 1995 run, they were placed in the target position indicated in Fig. 2a. In Table II, we list track- and dose-averaged LETs, percentage of dose contributed by iron particles, and percentage of dose from particles with LET > 100 keV/μm.

Figures 5a-f show several ϕ vs. LET spectra obtained behind sample holders; as a representative example, we describe some of

the features of Fig. 5b. In this case, a single polystyrene flask filled with cell-culture medium (designated as "*D*" in Table II) was placed on the beamline. Due to ionization energy loss in the flask, the energy of the surviving iron ions is slightly reduced, causing the LET peak to shift from 148 keV/μm to about 150 keV/μm. Several peaks, corresponding to ion species lighter than iron, are plainly visible in the histogram; the peak for manganese (Z = 25) is at about 139 keV/μm, on top of the low-end tail of the iron distribution from which it is barely distinguishable. Other peaks are visible down to Z = 12. We note that there is a slight preference for the production of even-Z nuclei, as can be seen from the (generally) higher peaks for those species compared to neighboring odd-Z nuclei. A similar trend is seen in other iron fragmentation data (7,10), including data presented below.

BEAM UNIFORMITY

In order to obtain an approximately uniform dose distribution over the entire sample surface, the radial and quadrantal dose distributions were monitored during the irradiations with the segmented ionization chambers. As was the case at the BEVALAC, the AGS beam transport system is optimized for a beam diameter on the order of 1 cm, which must be enlarged to several cm in order to irradiate most biological samples. At the BEVALAC, some defocusing of the beam was done using upstream magnets before the beam was finally transported through a set of thin lead foils; Coulomb multiple scattering in these foils served to spread the beam and enhance uniformity. At the AGS, all beam defocusing is done using upstream beamline magnets, which results in a coupling of the beam steering and beam profile.

Two distinct beam tunes were used for the biology experiments during the 1995 and 1996 runs at the AGS, referred to as low dose-rate (1-2 Gy per minute in 1995, 0.5 Gy per minute in 1996) and high dose-rate (8-10 Gy per minute in 1995, 12-15 Gy per minute in 1996) modes. Because most of the biological sample holders were no larger than 6 cm in any dimension, the dose distributions were optimized for uniformity on the four innermost rings, which cover this area. Over those rings, the dose in 1995 low dose-rate runs typically varied by ±2-3% relative to the ring 3 dose, which was used for the cutoff signal to the accelerator to stop the irradiation. The 1996 low dose-rate runs showed about ±7% variation over the innermost four rings, again relative to ring 3. For the high dose-rate runs, the dose varied by about ±6%, with little difference between the 1995 and 1996 runs.

INTERPRETATION OF THE BRAGG CURVE

The difference between the Bragg curves obtained at 1087 MeV/nucleon at the AGS and 600 MeV/nucleon at the BEVALAC is illustrated in the inset in Fig. 3, which covers the full range of water column depth used for the lower-energy beam. (A Bragg curve for the 610 MeV/nucleon iron beam at the AGS was obtained in 1996; it was nearly identical to that of the 600 MeV/nucleon beam at the BEVALAC.) We note that over the first 4 cm of water, there is little difference; at greater depths, the difference becomes quite pronounced, with the ratio rising for the lower-energy beam and falling for the higher-energy beam. Also, the ionization ratio peaks at about 4 for the 600 MeV/nucleon beam, in contrast to the peak ratio of slightly less than 1.0 for the 1087 MeV/nucleon beam.

There is a straightforward explanation for the differences between these depth/dose curves. As shown in Ref. (10), for a 600 MeV/nucleon beam and polyethylene targets, the track-averaged LET was nearly constant over the range of target depths from 0 to 5 cm, due to the offsetting effects of fragmentation and energy loss. Fragmentation produces ions lighter than

iron and hence with lower LET, whereas the velocity lost in traversing the target causes particles of all species to have higher LET at the exit than they did at the entrance. At 600 MeV/nucleon, the effects balanced each other almost exactly over the first 5 cm of polyethylene (4.6 g cm^{-2}). Only with an 8 cm target (7.3 g cm^{-2}) did the track-averaged LET increase, meaning that the velocity decrease was having a greater influence than the fragmentation. This explains the upturn in the Bragg curve seen at a similar depth of water. At 1087 MeV/nucleon, the energy loss curve is much flatter than it is at 600 MeV/nucleon[6], which partly explains the behavior of the Bragg curve at the AGS energy: the small increase in LET with depth is insufficient to balance the increasing fragmentation of the beam into lighter ions.

Calculations using the NUCFRG2 nuclear fragmentation model (16) show that the mean free path for fragmentation of iron in water is 10 cm; therefore at 29.7 cm (the range of the 1087 MeV/nucleon beam) only about 5% of the incident iron ions survive. In contrast, about 30% of the iron survives at 12 cm, the location of the Bragg peak for 600 MeV/nucleon. Regardless of energy, the fraction of surviving iron strongly influences the value of the ionization ratio in the peak of the Bragg curve, because the peak value is essentially an average (over a large number of particles and a wide range of LET) of the ratio for individual particles. Therefore it is not surprising that at 600 MeV/nucleon, where a substantial fraction of the incident iron survives, the peak in the Bragg curve is a factor of 4 higher than that in the 1087 MeV/nucleon curve, where very little iron survives.

The dose decreases monotonically with depth over the first 23 cm of H_2O with the 1087 MeV/nucleon beam. Over the first 12 cm of depth, the Bragg curve is well fit by a quadratic in depth given by $D(x) = 1.06 - .048x + .0012x^2$ where D is the dose relative to that at the upstream edge of the sample holder, and x is the depth in cm (or g cm^{-2}). The uniformity of dose across a sample thus degrades with increasing depth. For example, if a sample of 8 cm depth receives a dose of 1 Gy at the upstream edge, the dose in the center will be about 0.9 Gy and about 0.75 Gy at the downstream edge. Qualitatively speaking, the effects seen for the 1087 MeV/nucleon iron beam will be observed for any heavy ion beam of sufficient energy such that the position of the Bragg peak distance is substantially greater than the nuclear interaction mean free path. Experimenters working with thick samples and comparable beams should be aware of these effects.

FLUENCE RESULTS BEHIND CH_2 TARGETS

For $Z < 12$, the BEVALAC data suffered from inefficient triggering and the measured fluences were low by a large factor [which we estimated in Ref. (10) to be in the range 2-3, based upon a comparison to similar data obtained with CR-39 nuclear track detectors (17)]. In all lower-energy data sets, substantial acceptance corrections are needed at low Z. And in data sets C, E and F, clear peaks in the PSD2 spectra for individual fragment species are not clear below $Z = 12$. Thus, in the following, we restrict comparisons to the range $Z \geq 12$.

600 MeV/nucleon Fluence Measurements Compared

We begin by comparing data sets taken with similar beam energies. At the BEVALAC, materials upstream of the polyethylene targets degraded the nominal 600 MeV/nucleon beam to an energy of 510 MeV/nucleon at the target entrance. Largely because no lead scattering foils were used at the AGS, the 610 MeV/nucleon extraction energy is less degraded at the target entrance, to 555 MeV/nucleon according to our calculations. The two energies are sufficiently close to make a direct

comparison meaningful. After all corrections, we obtain the fluences shown in Table III and graphically in Fig. 6a. Uncertainties in the AGS data are much smaller than in the BEVALAC data, and have been suppressed in the plot in order to facilitate the comparison. The χ^2 between the two sets is 13.2 for 12 degrees of freedom; the agreement can therefore be said to be reasonably good. This tends to validate the (complicated) normalization procedures used in Ref. (10). Also, we find that the mean free path of iron ions is consistent between experiments — the BEVALAC data yield a value of 8.0 ± 0.5 g cm^{-2}, compared to 8.3 ± 0.2 g cm^{-2} at the AGS. We consider the AGS data to be more reliable, for reasons outlined above. Also shown in Fig. 6a (as a line) are the predictions of the transport model described in Ref. (15).

600 MeV/nucleon Fluences Compared to 1087 MeV/nucleon

With the 1087 MeV/nucleon beam energy at extraction, the iron energy at the target entrance was about 1050 MeV/nucleon. Table III and Figures 6b and c show the fluences obtained at the two beam energies. For the thinner target, we compare AGS data sets; for the thicker, AGS data are compared to BEVALAC data. Model predictions are shown for all cases.

The thin-target fluences shown in Fig. 6b vary slightly with beam energy, with more production of the heaviest fragments at the lower energy and more production of lighter fragments at the higher energy. Also at the higher energy, the mean free path for iron to undergo a nuclear interaction is 8.2 ± 0.2 g cm^{-2}, extremely close to the value obtained at the lower energy. Thus, the sum of fragment fluences in the range $12 \leq Z \leq 25$ is approximately independent of energy, while the individual fragment fluences show variations with energy.

For the thick-target fluences shown in Fig. 6c, the trend is the same, but the large error bars on the BEVALAC data preclude a definitive judgment. (The fluences for $20 \leq Z \leq 25$ are all higher at the lower energy.) At the higher energy, the mean free path for iron is found to be 8.2 ± 0.2 g cm^{-2}, at the lower energy, 7.9 ± 0.5 g cm^{-2}, again consistent with little or no energy dependence of the charge-changing nuclear cross section.

Thick-target Fluence at 1087 MeV/nucleon

A measurement behind 9.35 g cm^{-2} of polyethylene was made with the 1087 MeV/nucleon beam. Fluence results are shown in the far-right column of Table III. Comparing these fluences to those for data set E illustrates an interesting point: the increases in fluences of heavy fragments are suppressed at large target depth compared to the increases in fluences of lighter fragments. For instance, at 9.35 g cm^{-2}, ϕ for manganese ions is only 13% higher than at 4.68 g cm^{-2}, whereas ϕ for silicon ions ($Z = 14$) is 76% higher with the thicker target. This effect is due to secondary, tertiary and higher-order interactions in the target: the nuclear interaction cross sections increase with fragment mass, so that a greater proportion of heavy fragments interact than do light fragments. Further, these secondary and tertiary interactions tend to increase the yields of lighter fragments, since the interacting heavy secondaries "feed down" to produce lighter fragments, an effect which increases with target depth. These data demonstrate the importance of multiple interactions in heavy-ion transport models.

Neutrons are expected to be copiously produced behind thick targets, but at the depths used here, both fluence and dose are dominated by charged particles. Only at substantially greater depths, where ionization energy loss causes most or all of the charged particles to stop in the target material, does the neutron dose become

important. We note that the detector systems used in the present measurements are largely insensitive to neutrons.

Comparisons Between Data and Model

As shown in Figs. 6a and 6c, and described in Ref. (15), for the 600 MeV/nucleon Fe beams, the model predicts a higher fluence of the heaviest fragments ($22 \leq Z \leq 25$) than is measured; the discrepancy is most pronounced for Cr ($Z = 24$). For the 1.94 g cm^{-2} data, the model is in good agreement with the data over the rest of the spectrum, while at 4.68 g cm^{-2}, the model-predicted fragment fluences are generally lower than the data. The data show an enhancement in fluence for even-Z ions which is not predicted by the model. In Fig. 6b and 6c, the model predictions for the higher-energy beam are in excellent agreement with the data. These results suggest that the NUCFRG2 part of the code, which calculates the fragmentation cross sections, needs adjustment in its energy-dependent portions.

Track-Averaged LETs Behind Polyethylene in 1087 MeV/nucleon Spectra

We previously reported track-averaged LET's of 166, 162, 167 and 216 keV/μm for our BEVALAC data behind 0, 1.82, 4.55 and 7.28 g cm^{-2} of polyethylene, respectively. If we take ratios of the non-zero depth values to the zero-depth value, we obtain .98, 1.01 and 1.30. When these points are compared to the Bragg curve for this beam (shown as an inset in Fig. 3), they fall quite near the actual Bragg curve data for this beam energy. Similarly, the 1087 MeV/nucleon AGS polyethylene data yield track-averaged LETs of 147, 135, 117 and 95 keV/μm for target-out, 1.94, 4.68 and 9.35 g cm^{-2} of polyethylene, respectively. Divided by the target-out value, these values are .92, .80, and .65; and, as was true for the 600 MeV/nucleon beam, these points fall quite near the corresponding Bragg curve data. The correspondence between track-averaged LET (relative to the LET of the primary ion) and the value of the Bragg curve at a particular depth allows one to infer, at least approximately, the water-equivalent depths of the biolgy sample holders, using the track-averaged LET values in Table II (divided by the LET of the unmodified beam) and the Bragg curve in Fig. 3. (The quadratic fit of dose vs. depth given above may be useful here.)

CONCLUSIONS

We have measured several important quantities related to 1087 MeV/nucleon ^{56}Fe beams used for radiobiology at the BNL AGS, including depth-dose distribution, and track- and dose-averaged LET of the beam at the entrance and exit of biological sample holders. Some beam characteristics are significantly different from those of the 600 MeV/nucleon energy beams used in similar experiments at the LBL BEVALAC. The respective Bragg curves show the strong effects of the interplay between ionization energy loss and nuclear fragmentation as a function of beam energy, which must be accounted for in planning biological irradiations, especially of thick samples. Fluence spectra for $12 \leq Z \leq 25$ obtained at the AGS behind polyethylene have been reported and compared to previous BEVALAC measurements, demonstrating good agreement for similar data and showing the energy dependence of the fluences. The data were also compared to a transport model and show good agreement over most of the range of fragment charge.

ACKNOWLEDGMENTS

Many individuals at LBNL and in the BNL AGS, Biology and Medical departments contributed to the success of the AGS radiobiology runs, and we particularly thank D. Lazarus and W. McGahern of the AGS staff for their outstanding technical and logistical support. We are indebted to B.

Ludewigt, M. Nyman and especially R. P. Singh of LBNL for generous donations of their time and expertise with the dosimetry system. We are grateful to W. Schimmerling of the NASA Space Radiation Health Program for his long-time support and encouragement of this program. We thank T. Borak and S. Rademacher of Colorado State University, and T. Carter and C. Stronach of Virginia State University, for their help in putting the experiment together. We appreciate the assistance given by A. Kronenberg of LBNL in editing this manuscript. This work was supported at LBNL by the NASA Space Radiation Health Program under NASA Grant L14230C through the U.S. Department of Energy under Contract No. DE-AC03076SF00098.

FOOTNOTES

1. The simple proportionality relationship between charge collected in the IC's and dose in water relies on the assumptions that beam particles are not stopping in the chambers, and that the chambers are in electron equilibrium. The latter may not be perfectly valid at high beam energies, where high-energy delta rays can be produced. This lack of perfect equilibrium may contribute to the observed 8% discrepancy between IC and "egg" chamber doses.

2. Particle identification in our AGS data is simpler than in our BEVALAC data because: (1) at higher beam energies like 1087 MeV/nucleon, the ΔE spectrum of any particular fragment species is a distinct Gaussian distribution which is well-separated from the Gaussians due to other fragment species; (2) with the 610 MeV/nucleon AGS beam, relatively thin targets were used so that the separation between Gaussians remained good; (3) improved triggering allows us to see the entire spectrum of fragments with good statistics.

3. We refer throughout to planar fluence. In the context of the beam characterization data, unit incident fluence is a single beam particle which deposited energy in the trigger detectors (T1 and T2 in 1995, d3mm1 and d3mm2 in 1996) sufficient to fire the trigger. In the context of the measurements behind polyethylene, unit incident fluence is a single iron particle incident on the target.

4. The energy loss calculations were performed by numerical integration of the Bethe-Bloch equation (9) using an appropriately small step size. We note that at 1087 MeV/nucleon, the density effect is significant and must be taken into account. This is not the case at 600 MeV/nucleon.

5. In the 1995 data, with very few events below 20 keV/μm, the track-averaged LET is found to be 142 keV/μm, the dose-averaged LET 147 keV/μm. As a check of consistency between the 1995 and 1996 data, we calculated track- and dose-averaged LET values using the 1996 data but including only the particles with LET > 20 keV/μm; the resulting values were within 1% of those obtained with the 1995 data.

6. For an illustration, see the curves on pg. 132 of Ref. (14).

REFERENCES

1. Space Studies Board, National Research Council, *Radiation Hazards to Crews of Interplanetary Missions*, National Academy Press, Washington, D.C. (1996).

2. T.C. Yang, L.M. Craise, M.-T. Mei and C.A. Tobias, Neoplastic Cell Transformation by Heavy Charged Particles. *Radiat. Res.* **104**, S177-S187 (1985).

3. S.M.J. Afzal and E.J. Ainsworth, Radioprotection of Mouse Colony-Forming Units-Spleen against Heavy Charged Particle Damage by WR 2721. *Radiat. Res.* **109**, 118-126 (1987).

4. K. Tsuboi, T.C. Yang and D.J. Chen, Charged-Particle Mutagenesis, I. Cytotoxic and Mutagenic Effects of High-LET Charged Iron Particles on Human Skin Fibroblasts. *Radiat. Res.* **129**, 171-176 (1992).

5. E.L. Alpen, P. Powers-Risius, S.B. Curtis and R.J. DeGuzman, Tumorigenic Potential of High-Z, High-LET Charged-Particle Radiations. *Radiat. Res.* **136**, 382-391 (1993).

6. C. Medvedovsky, B.V. Worgul, Y. Huang, D.J. Brenner, F. Tao, J. Miller, C. Zeitlin and E.J. Ainsworth, The Influence of Dose, Dose Rate and Particle Fragmentation on Cataract Induction by Energetic Iron Ions, *Adv. Space Res.* **14**, 475 (1994).

7. C. Zeitlin, L. Heilbronn, J. Miller, S. E. Rademacher, T. Borak, T. R. Carter, K. A. Frankel, W. Schimmerling and C. E. Stronach, Heavy fragment production cross sections from 1.05 GeV/nucleon ^{56}Fe in C, Al, Cu, Pb and CH_2 targets, *Phys. Rev. C* **56,** 388-397 (1997).

8. International Commission on Radiation Units and Measurements, *Linear Energy Transfer*, Report No. 16., ICRU, Bethesda, Maryland (1970).

9. C. Zeitlin, K. A. Frankel, W. Gong, L. Heilbronn, E. J. Lampo, R. Leres, J. Miller and W. Schimmerling, A modular solid state detector for measuring high energy heavy ion fragmentation near the beam axis, *Radiat. Meas.* **23**, 65-81 (1994).

10. C. Zeitlin, L. Heilbronn, J. Miller, L. Heilbronn, K. Frankel, W. Gong and W. Schimmerling, The fragmentation of 510 MeV/nucleon Iron-56 in polyethylene. I. Fragment fluence spectra, *Radiat. Res.* **145**, 655-665 (1996).

11. A. S. Goldhaber, Statistical models of fragmentation processes, *Phys. Lett.* **53B**, 306 (1974).

12. R. K. Tripathi and L. W. Townsend, Simple parameterization of fragment reduced widths in heavy ion collisions, *Phys. Rev. C* **49**, 2237 (1994).

13. International Commission on Radiation Units and Measurements, *Stopping Powers and Ranges for Protons and Alpha Particles*, Report No. 49, ICRU, Bethesda, Maryland (1993).

14. Particle Data Group, "Review of Particle Properties", *Phys. Rev. D* **54**, (1996).

15. C. Zeitlin, L. Heilbronn, J. Miller, L. Heilbronn, W. Schimmerling, L. W. Townsend, R. K. Tripathi and J. W. Wilson, The fragmentation of 510 MeV/nucleon Iron-56 in polyethylene. II. Comparisons between data and a model. *Radiat. Res.* **145**, 666-672 (1996).

16. J. W. Wilson, J. L. Shinn, L. W. Townsend, R. K. Tripathi, F. F. Badavi and S. Y. Chun, NUCFRG2: A semiempirical nuclear fragmentation model, *Nucl. Instr. Meth. B***94**, 95-102 (1994).

17. J. L. Shinn, J. W. Wilson, F. F. Badavi, E.V. Benton, I. Csige, A. L. Frank and E. R. Benton, HZE beam transport in multilayered materials, *Radiat. Meas.* **23**, 57-64 (1994).

FIGURE CAPTIONS

1. Schematic diagrams of the arrangements of parallel-plate ionization chambers: a. in the sample irradiation configuration, and b. in the Bragg curve measurement configuration.

2. Schematic diagrams of silicon detector system used to make particle fluence measurements. a. The 1995 arrangement. b. The 1996 arrangement used for beam characterization studies. c. The 1996 configuration used for measurements behind polyethylene with the 610 MeV/nucleon beam.

3. Bragg curve for 1087 MeV/nucleon ^{56}Fe, using data from ring 1, the innermost ring in the IC's. The inset figure shows the Bragg curve obtained with a 600 MeV/nucleon beam at the BEVALAC, and the 1087 MeV/nucleon beam over the same depth of water.

4a. Fluence vs. LET of the "raw" beam (i.e., as seen at the exit window), obtained with the 1996 data. 4b. Dose vs. LET based on Fig. 4a, as described in the text. 4c. Integral of dose vs. LET. The plotted quantity is, for the i$^{\text{th}}$ bin, $\sum_{i=1}^{L_i} D(L_i) \Big/ \sum_{j=1}^{180} D(L_j)$ where the summation runs over the bins of the histogram show in Fig. 4b.

5. Fluence vs. LET measured behind several sample holders. The correspondence between the figure label and sample holder designation in Table II is as follows: Fig. 5a, sample holder *C*; 5b, *D*; 5c, *G*; 5d, *H*; 5e, *L*; and 5f, *N*.

6. Fragment fluences behind polyethylene targets. From top to bottom, the plots show the results behind: a. 1.94 g cm^{-2} for 600 MeV/nucleon (at extraction) iron beams at the BEVALAC and at the AGS; b. 1.94 g cm^{-2} at the AGS at two beam energies; c. 4.68 g cm^{-2} for the 600 MeV/nucleon iron beam at the BEVALAC and the 1087 MeV/nucleon AGS beam. Model predictions are shown as lines.

TABLE I
Data Sets With Iron On Polyethylene

Energy at target entrance(MeV/nucleon)	Target Depth (g cm^{-2})	Year Taken	Designation	Detector Acceptance Angle
510	1.82	1992	A	1.5°
555	1.94	1996	B	2.0°
1050	1.94	1995	C	3.5°
510	4.55	1992	D	1.5°
1050	4.68	1995	E	3.5°
1050	9.35	1995	F	3.5°
510	7.28	1992	G	1.5°

TABLE II
Track- and Dose-Averaged LETs and Fe Dose Fractions Behind Sample Holders

	Sample Holder Designation and Description	$\overline{LET}_{trk}$ keV/μm (note 1)	$\overline{LET}_{dose}$ keV/μm (note 2)	% of Dose, L > 140 keV/μm	% of Dose, L > 100 keV/μm
A	none	112	145	94	97
B	Falcon T-25, 1 side	110	145	94	97
C	Falcon T-25, 2 sides, empty	109	145	93	97
D	Falcon T-25, filled	100	143	86	93
E	Falcon T-25, filled+ 1 side	100	143	85	93
F	Falcon T-75, filled	93	142	83	92
G	Corning 25 cm^2, 25100-25	98	143	86	93
H	(Corning 25 cm^2, 25100-25)× 2	90	140	78	89
I	Corning 60-mm tissue culture dish, #25010	106	145	93	97
J	tapered cylindrical beaker[3], empty	108	145	93	97
K	cylindrical beaker[3], water-filled	86	138	74	87
L	Fisher 1013 petri dish, filled	109	146	93	97
M	(Fisher 1013 petri dish, filled)× 2	107	146	91	96
N	(Fisher 1013 petri dish, filled)× 3	104	144	88	95

Notes. 1. Track-averaged LET values have uncertainties of approximately ±3% (see text). 2. Dose-averaged LET values have uncertainties of approximately ±1%. 3. Cylinder is polyproylene, with dimensions as follows: height, 10 cm; diameter at top, 8 cm; diameter at bottom, 6.5 cm.

TABLE III

Corrected Fragment Fluences ($\times 10^3$) Behind Polyethylene Targets

Z	1.94, 510	1.94, 555	1.94, 1050	4.68, 510	4.68, 1050	9.35, 1050
25	25.0 ± 3.1	29.2 ± 0.7	25.5 ± 0.5	45.0 ± 3.6	42.8 ± 1.1	49.7 ± 1.1
24	21.7 ± 3.0	25.0 ± 0.5	20.0 ± 0.4	39.5 ± 3.0	37.3 ± 1.0	44.5 ± 1.0
23	15.7 ± 2.6	16.9 ± 0.4	15.7 ± 0.4	31.8 ± 3.0	27.7 ± 0.9	38.0 ± 0.9
22	14.6 ± 2.4	16.7 ± 0.4	15.7 ± 0.4	29.9 ± 3.0	29.6 ± 0.9	40.0 ± 0.9
21	11.7 ± 1.8	12.3 ± 0.4	12.6 ± 0.3	23.3 ± 1.8	22.5 ± 0.8	32.7 ± 0.9
20	13.0 ± 1.8	10.5 ± 0.4	11.8 ± 0.3	24.7 ± 1.9	23.3 ± 0.8	35.8 ± 0.9
19	8.0 ± 1.7	8.2 ± 0.3	8.9 ± 0.3	17.8 ± 1.9	19.0 ± 0.7	27.5 ± 0.8
18	8.0 ± 1.5	7.1 ± 0.3	9.0 ± 0.3	16.2 ± 1.5	18.5 ± 0.7	28.5 ± 0.8
17	5.7 ± 1.6	5.6 ± 0.3	7.5 ± 0.3	13.9 ± 1.7	15.6 ± 0.6	22.9 ± 0.7
16	6.5 ± 1.7	5.3 ± 0.3	7.6 ± 0.3	18.5 ± 1.8	15.9 ± 0.6	26.3 ± 0.8
15	6.1 ± 1.4	4.3 ± 0.3	5.7 ± 0.2	12.6 ± 1.5	12.3 ± 0.6	21.8 ± 0.7
14	4.3 ± 2.3	5.3 ± 0.4	7.4 ± 0.5	14.9 ± 2.5	15.8 ± 0.6	27.8 ± 0.8
13	7.1 ± 1.5	3.9 ± 0.3	5.6 ± 0.3	13.0 ± 1.5	12.4 ± 0.6	22.6 ± 0.7
12	3.1 ± 1.8	4.5 ± 0.4	5.0 ± 0.3	12.3 ± 2.8	12.9 ± 0.6	20.4 ± 0.7

Notes. Fluences are per incident Fe ion. Numbers in column headings separated by commas are target areal density in g cm^{-2} and beam energy at target entrance in MeV/nucleon. Fluences for data set G are reported in Ref. (10).

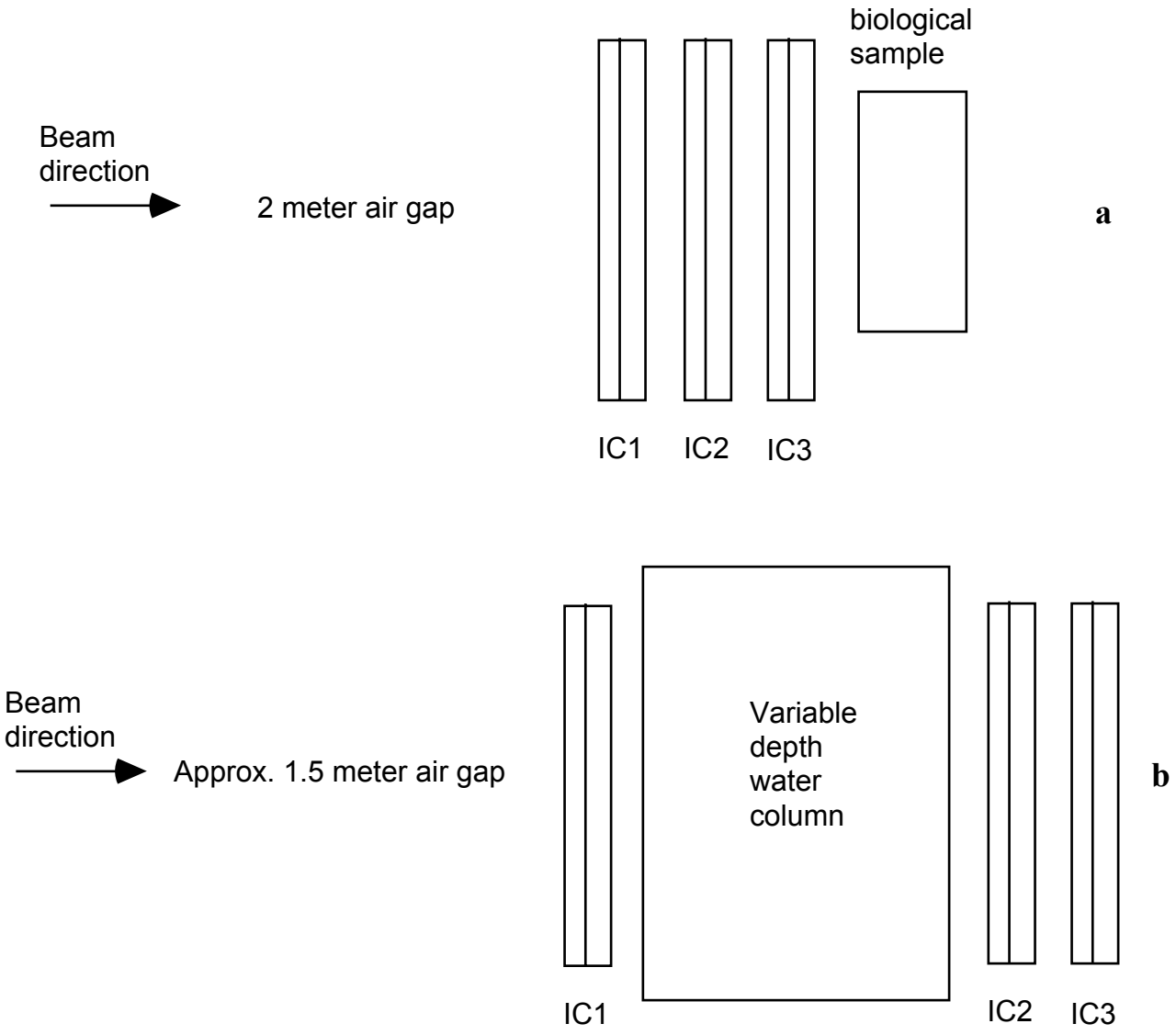
biological
sample
Beam
direction
2 meter air gap
a
IC1
IC2
IC3
Beam
direction
Approx. 1.5 meter air gap
Variable
depth
water
column
b
IC1
IC2
IC3

Figure 1

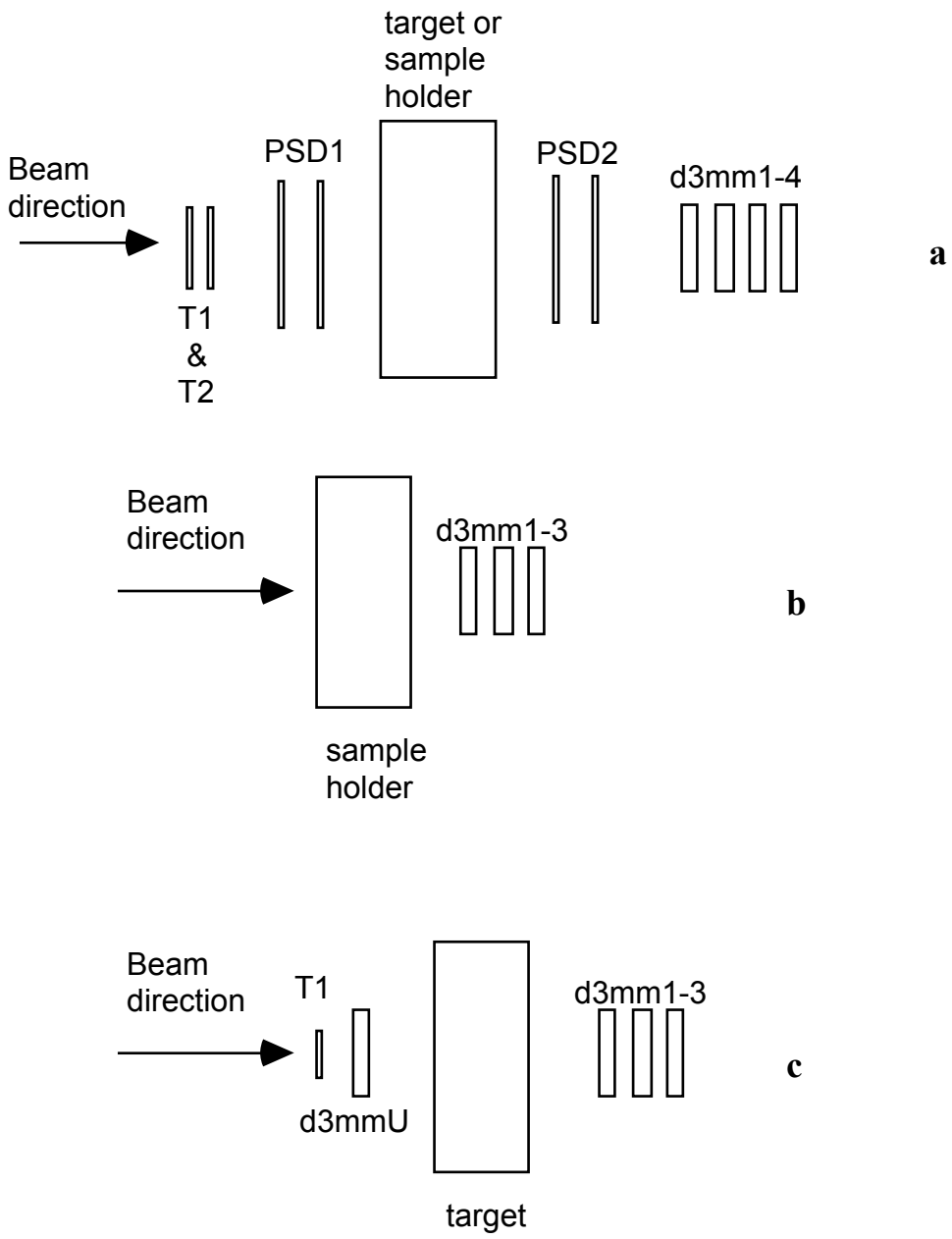
target or
sample
holder
Beam
direction
PSD1
PSD2
d3mm1-4
T1
&
T2
a
Beam
direction
d3mm1-3
b
sample
holder
Beam
direction
T1
d3mm1-3
d3mmU
c
target

Figure 2

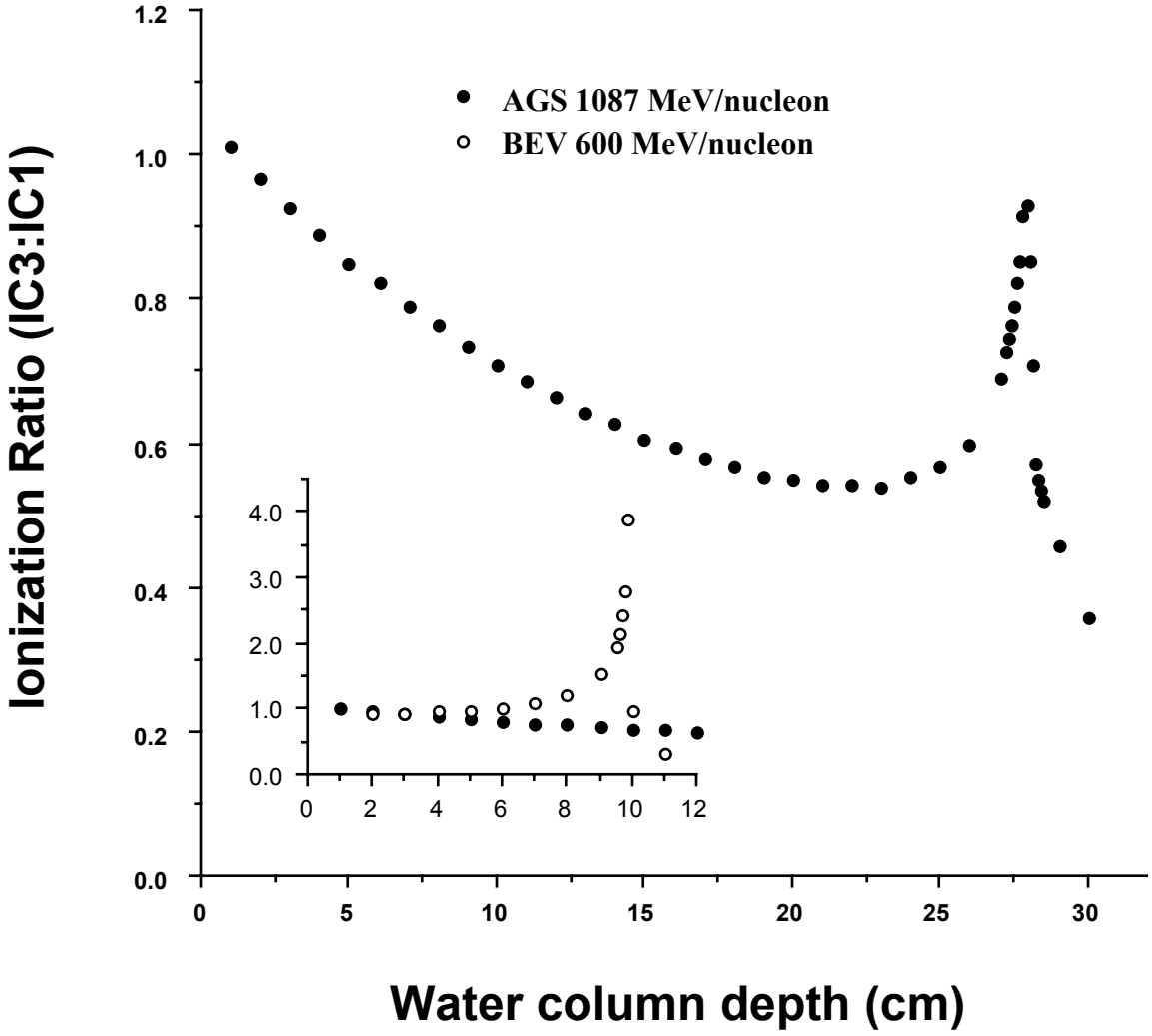
AGS 1087 MeV/nucleon
BEV 600 MeV/nucleon
Ionization Ratio (IC3:IC1)
Water column depth (cm)
1.2
1.0
0.8
0.6
0.4
0.2
0.0
0
5
10
15
20
25
30
4.0
3.0
2.0
1.0
0.0
0
2
4
6
8
10
12

Figure 3

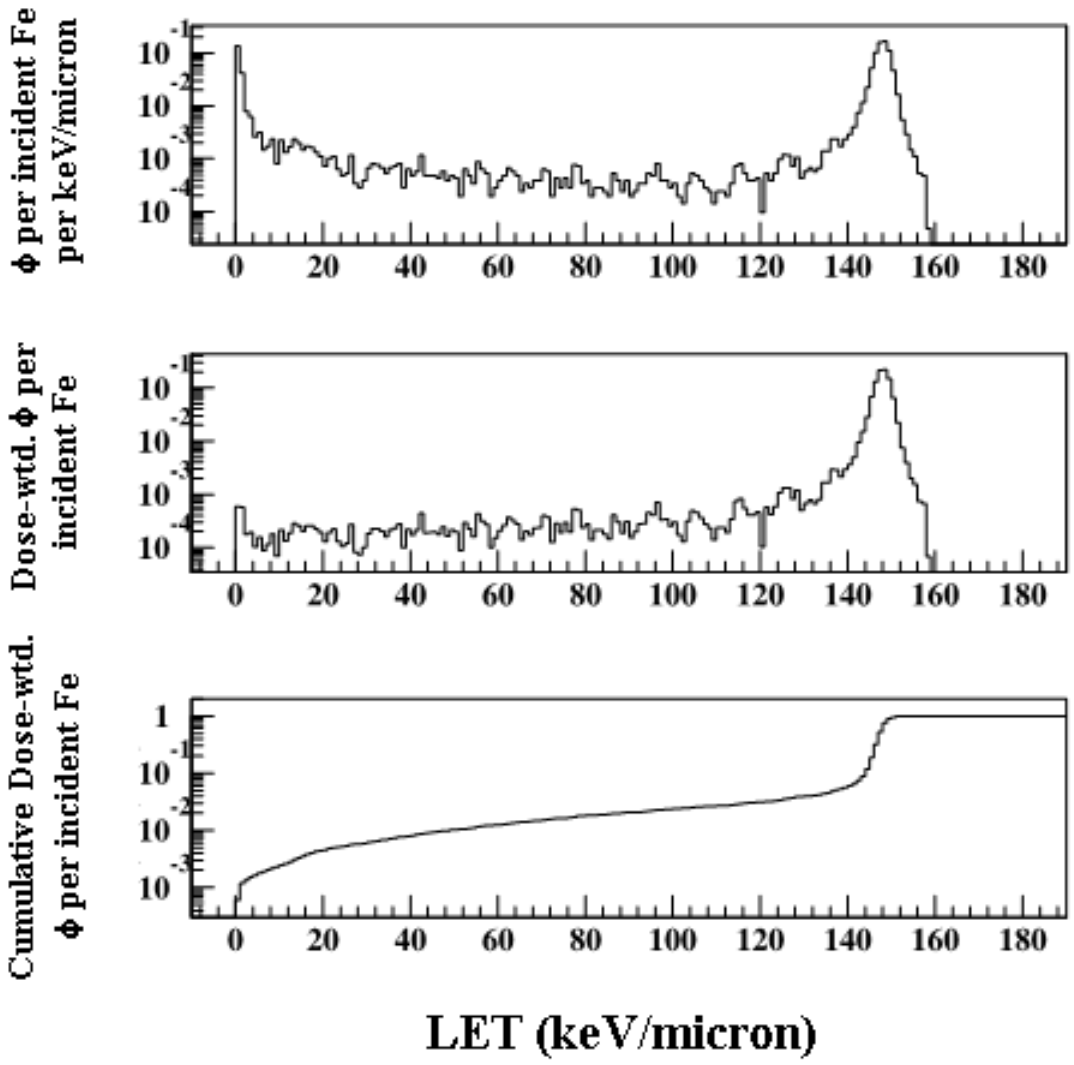
ϕ per incident Fe per keV/micron
Dose-wtd. ϕ per incident Fe
Cumulative Dose-wtd. ϕ per incident Fe
0
20
40
60
80
100
120
140
160
180
LET (keV/micron)

Figure 4

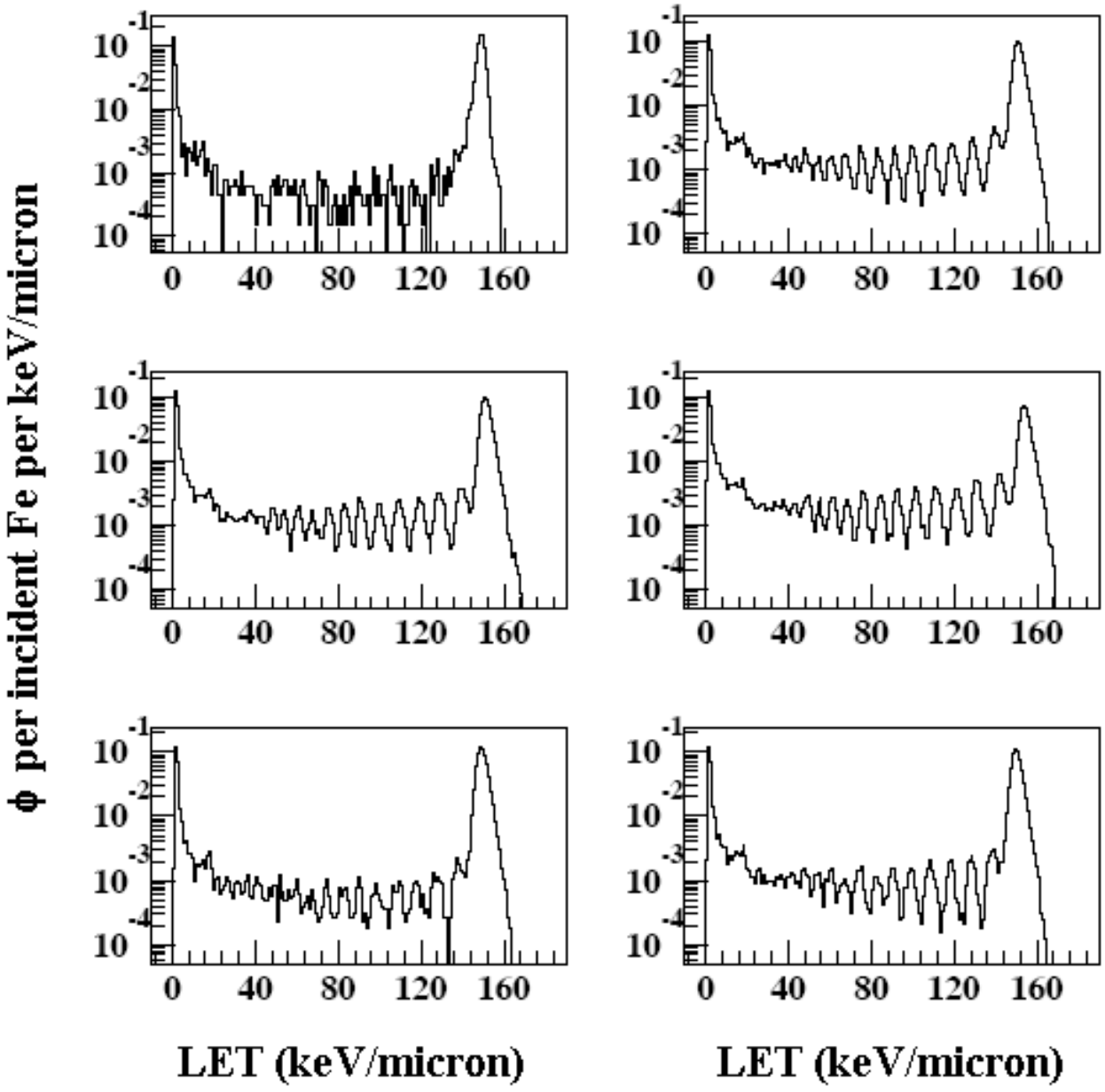
ϕ per incident Fe per keV/micron
10^-1
10^-2
10^-3
10^-4
0
40
80
120
160
LET (keV/micron)
LET (keV/micron)

Figure 5

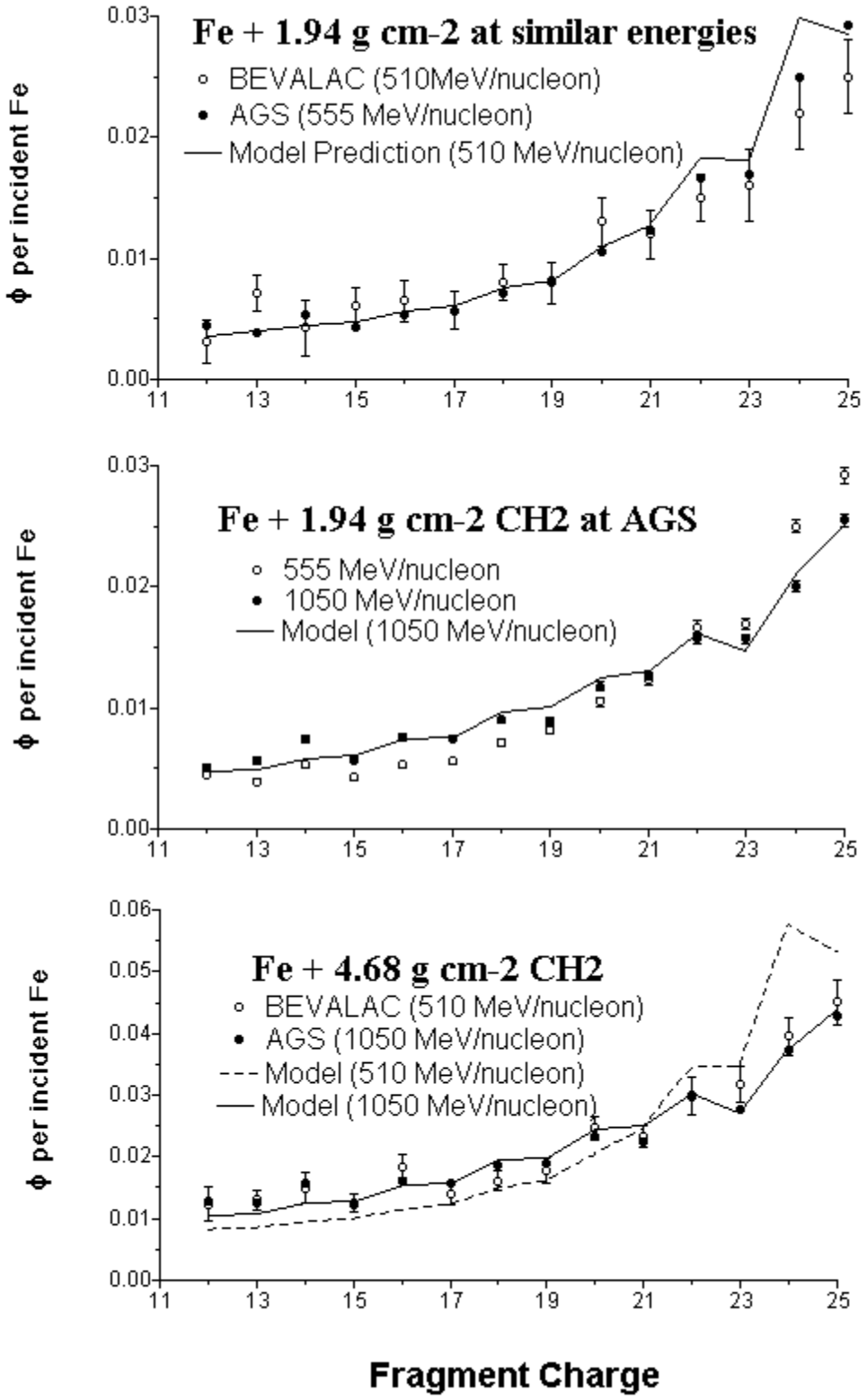
Fe + 1.94 g cm-2 at similar energies
BEVALAC (510MeV/nucleon)
AGS (555 MeV/nucleon)
Model Prediction (510 MeV/nucleon)
Fe + 1.94 g cm-2 CH2 at AGS
555 MeV/nucleon
1050 MeV/nucleon
Model (1050 MeV/nucleon)
Fe + 4.68 g cm-2 CH2
BEVALAC (510 MeV/nucleon)
AGS (1050 MeV/nucleon)
Model (510 MeV/nucleon)
Model (1050 MeV/nucleon)
ϕ per incident Fe
Fragment Charge

Figure 6